SCIENTIFIC REP🞓RTS

OPEN

Mechanisms-based viscoplasticity: Theoretical approach and experimental validation for steel 304L

Aleksander Zubelewicz[1] & Wiera Oliferuk[2]

We propose a mechanisms-based viscoplasticity approach for metals and alloys. First, we derive a stochastic model for thermally-activated motion of dislocations and, then, introduce power-law flow rules. The overall plastic deformation includes local plastic slip events taken with an appropriate weight assigned to each angle of the plane misorientation from the direction of maximum shear stress. As deformation progresses, the material experiences successive reorganizations of the slip systems. The microstructural evolution causes that a portion of energy expended on plastic deformation is dissipated and the rest is stored in the defect structures. We show that the reorganizations are stable in a homogeneously deformed material. The concept is tested for steel 304L, where we reproduce experimentally obtained stress-strain responses, we construct the Frost-Ashby deformation map and predict the rate of the energy storage. The storage is assessed in terms of synchronized measurements of temperature and displacement distributions on the specimen surface during tensile loading.

Despite significant advances in modeling the inelastic behavior of polycrystalline materials, our understanding of the deformation mechanisms is still incomplete. Temperature, strain rate and strain range alter mechanical properties of the materials, shift the source of the material's nonlinearity within different levels of the internal structure, thus making the behavior hierarchical in nature[1]. At early stages of plastic deformation, dislocations nucleate, multiply and move freely within grains. As the deformation process continues, grain boundaries and other defects obstruct the dislocation mobility. We know that plastic work is not fully dissipated and a measurable portion of it adds to internal energy of the deformed materials. This energy has been discovered in calorimetric tests performed by Taylor and Quinney[2]. For many years, based on their work, the part of the work converted to internal energy and stored in the metallic material has been considered to be a constant value of about ten percent of the entire plastic work. Further experimental studies have shown that this estimation is wrong[3–7] and, in fact, the ratio of the energy is not constant and depends on the deformation level of the tested material. Consequently, a concept of the energy storage rate is proposed[8–11]. The stored energy results from the evolution of the microstructure and is an essential measure of its cold work state[12]. Consequently, the microstructural reorganizations increase internal energy of the material. The energy storage is often mitigated by a partial restoration of the grain shape due to the relaxation of dislocation pileups, dynamic recrystallization and/or grain boundary sliding.

Since seventies, constitutive modeling is steadily migrating from purely phenomenological descriptions toward the approaches which are based on micromechanics considerations. The phenomenology means that the models offer reliable responses but only within the domain already verified by experiment. Often, extrapolation of the behavior to the regimes not tested can be troublesome. The introduction of crystal plasticity approaches[13–15] significantly improves the predictability by correctly specifying the mechanisms of plastic slip. In our approach, we attempt to bridge the benefits of the phenomenology with the advantages of the micromechanics based descriptions. The study consist of four sections. First, we develop a generalized concept of the thermally activated motion of dislocation. Next, we propose a Tresca-type stochastic concept, where the dominant plastic deformation is collected from slip systems placed on the plane defined by the maximum and minimum principal stresses. As a result, we introduce an average Schmid factor. The factor encapsulates the relevant information about the evolving configuration of the active systems. Also, we provide a micromechanisms-based interpretation of the

[1]University of New Mexico, Civil Engineering, Albuquerque, NM, USA. [2]Bialystok University of Technology, Bialystok, Poland. Correspondence and requests for materials should be addressed to A.Z. (email: alek@unm.edu)

energy storage rate. We point into the conditions, at which the microstructural evolution may become unstable. Lastly, we introduce a visco-plasticity model capable of capturing metal responses within a broad range of strain rates and temperatures.

Results

Notation. Dyadic product: **n n** corresponds to $n_i n_j$, where in Cartesian coordinate system $i, j = 1, 3$

Inner product of second order tensors: $\boldsymbol{\sigma} : \dot{\mathbf{H}}^p$ is $\sigma_{ij} \dot{H}_{ij}^p$

Product of tensors: $\mathbf{C} \cdot \dot{\mathbf{H}}^e$ is $C_{ijkl} \dot{H}_{kl}^e$

Thermally activated motion of dislocations. The thermally activated motion of dislocations and subsequent dislocation interactions are reflected in activation free energy $F_a = E_a - S_a T$, where E_a and S_a are the activation energy and activation entropy[16]. We introduce the non-dimensional function $\xi_a = F_a / k_b T$, where k_b is Boltzmann constant and T is temperature. The processes are stochastic with respect to ξ_a and, therefore, frequency of the dislocation-triggered events follows a statistical distribution and is assumed here to be the Weibull distribution $f_D = k_a \xi_a^{k_a - 1} \exp[-\xi_a^{k_a}]$. An increase in the entropic contribution $S_a T$ makes the material softer and strength is reduced. The material is expected to experience the events with a frequency $f_D(T)$ and with the rate defined by the exponent k_a. In a collective sense, the dislocation activities at temperature T include all the events available up to this temperature with the appropriate frequencies. These events effectively reduce the material's resistance to plastic flow. Therefore, the actual resistance A_D is integrated over the frequencies in the domain taken between T_c/T_m and T_c/T and, then, we have $A_D = \int_{T_c/T_m}^{T_c/T} f_D(s)\,ds$. The variable s defines the pathway of temperature T_c/T. The activation factor A_D is a measure of thermal softening. At temperatures higher from the transition temperature T_c the material becomes increasingly softer and its strain rate sensitivity increases. Often, the transition occurs at temperature close to $T_m/3$, where T_m is melting temperature. In here, the activation energy is expressed in terms of $k_b T_c$ such that $E_a = g_a^{1/k_a} k_b T_c$. When entropy is assumed to be weakly dependent on temperature, then at melting point $F_a(T_m) = 0$ we have $S_a = E_a/T_m$. Consequently, the activation factor becomes

$$A_D(T) = 1 - exp\left[-g_a\left(\frac{T_c}{T} - \frac{T_c}{T_m}\right)^{k_a}\right],$$

(1)

where g_a determines the magnitude of the activation energy. At the solidus temperature, where $A_D(T_m) \to 0$, the dislocation activities are replaced by diffusional flow. At very low temperature, the factor A_D is only slightly smaller from one and the material exhibits high resistance to plastic deformation.

Deformation-induced slip reorganization. In the Tresca-like material, the macroscopically observed plastic strain rate $\dot{\mathbf{H}}^p$ follows the direction of maximum shear stress and is

$$\dot{\mathbf{H}}^p = \frac{1}{2}\mathbf{N}^\sigma \dot{e}^p.$$

(2)

The magnitude of the plastic strain rate $\dot{e}^p$ is affected not only by shear stress and temperature but also is sensitive to the evolving slip configuration. Components of the strain rate $\dot{\mathbf{H}}^p$ are defined in terms of the dyadic product $\mathbf{N}^\sigma = (\mathbf{n}^\sigma \mathbf{s}^\sigma + \mathbf{s}^\sigma \mathbf{n}^\sigma)$. The unite vectors $\mathbf{n}^\sigma$ and $\mathbf{s}^\sigma$ are orthogonal and are determined by the current stress $\boldsymbol{\sigma}$. We construct the stress representation $\mathbf{N}^\sigma = \mathbf{N}^\sigma(\boldsymbol{\sigma})$, which must retain the properties of the dyadic product $(\mathbf{n}^\sigma \mathbf{s}^\sigma + \mathbf{s}^\sigma \mathbf{n}^\sigma)$, thus $tr\mathbf{N}^\sigma = 0$, $tr(\mathbf{N}^\sigma)^2 = 2$ and $\mathbf{N}^\sigma = (\mathbf{N}^\sigma)^3$. This expression has already been derived[17] and is

$$\mathbf{N}^\sigma = \frac{2 \cos\frac{\varphi}{3}}{\sqrt{3} \cos\varphi}\left(\mathbf{1} - \frac{3}{2 J_2}\mathbf{S}^2\right) + \frac{\cos\frac{2\varphi}{3}}{\sqrt{J_2} \cos\varphi}\mathbf{S},$$

(3)

where the angle is $\varphi = \sin^{-1}(J_3\sqrt{27/4}\,/\,J_2^3)$. The second and third invariants of stress deviator $\mathbf{S} = \boldsymbol{\sigma} - \mathbf{1}\,tr\,\boldsymbol{\sigma}/3)$ are J_2 and J_3. Note that the expression produces singular responses when the angle φ approaches the values $\pm\pi/2$. These points correspond to the corners on the Tresca stress envelop.

Plastic deformation is collected from many slip planes with orientations distributed around the plane of maximum shear stress. Each such θ-active plane is defined in terms of orthogonal triad $\{\mathbf{n}^\theta, \mathbf{s}^\theta, \mathbf{m}^\theta\}$, where identity tensor is $\mathbf{1} = \mathbf{n}^\theta \mathbf{n}^\theta + \mathbf{s}^\theta \mathbf{s}^\theta + \mathbf{m}^\theta \mathbf{m}^\theta$ and slip occurs on the planes defined by the unite vectors $\mathbf{n}^\theta$ and $\mathbf{s}^\theta$. Plastic deformation in each grain is sensitive to the grain orientation and is dependent on the grain size and shape. Incoherencies of the deformation at grain boundaries and in the presence of other defects permanently distort the lattice and are responsible for an increase of internal energy. Consequently, these incoherencies in a plastically deformed material broaden the angular spectrum of the active slip systems. It is worth noting that at large plastic deformation the spectrum tightens again[18] and the material may experience localized plastic deformation. In here, we narrow the study to the conditions, where the localized shear bands are not present. Further discussion on the conditions, which lead to the formation of shear bands, is presented in the next section. The vectors $\mathbf{n}^\theta$ and $\mathbf{s}^\theta$ and their rotations occur on the plane defined by the maximum and minimum principal stresses. The θ-planes undergo rotations such that
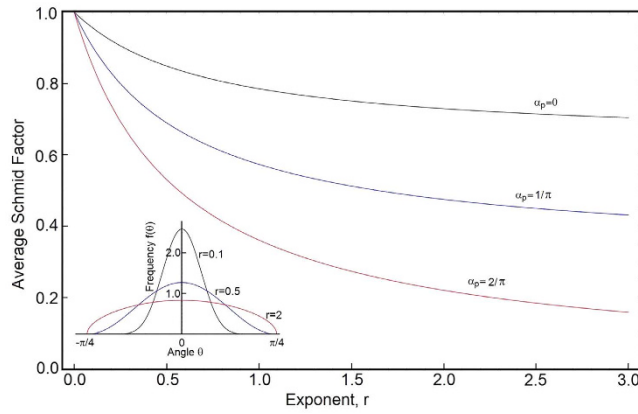
Figure 1. The average Schmid factor M specifies flow constraints, which result from the current orientation of slip systems M_s and is sensitive to the reorientations M_r. The factor is plotted as a function of the exponent r and is shown for three rates of slip reconfigurations $\alpha_p = 0, \quad 1/\pi$ and $2/\pi$. Three shapes of the distribution $f_\theta(\theta)$ are presented for exponents $r = 0.1, 0.5$ and 2.

$$\begin{Bmatrix} \dot{\mathbf{n}}^\theta \\ \dot{\mathbf{s}}^\theta \end{Bmatrix} = \begin{bmatrix} 0 & \dot{\theta} \\ -\dot{\theta} & 0 \end{bmatrix} \begin{Bmatrix} \mathbf{n}^\theta \\ \mathbf{s}^\theta \end{Bmatrix}. \tag{4}$$

The plastic strain rate $\dot{\mathbf{H}}^p$ incorporates slip rates from the entire spectrum of the slip orientations, where the slip contributions vary and depend on the current angle θ. In the representative volume of the materials, we have a large number of such systems and, therefore, we assume that the orientations are continuously distributed about the plane of maximum shear stress. The distribution $f_\theta(\theta)$ of the slip contributions is taken for angles between $\pm\pi/4$. The form of the distribution is sufficiently general when constructed as follows

$$f_\theta(\theta) = \frac{2\Gamma(1 + 1/2r)}{\sqrt{\pi}\ \Gamma(1/2 + 1/2r)}\ \cos^{1/r} 2\theta, \tag{5}$$

where we assure that $\int_{-\pi/4}^{\pi/4} f_\theta(\theta)d\theta = 1$ and Γ is gamma function. The exponent r determines the shape of the distribution. We note that the larger the exponent is the broader the distribution becomes, Fig. 1. At advanced deformation, the slip systems sense each other, interact with grain boundaries and other defects. Consequently, the interactions widen the distribution and create the conditions for plastic hardening. At the microscale, the rate of plastic strain $\dot{\mathbf{H}}^p$ is defined as

$$\dot{\mathbf{H}}^p = \frac{1}{2} \int_{-\pi/4}^{\pi/4} \frac{\partial[(\mathbf{n}^\theta\mathbf{s}^\theta + \mathbf{s}^\theta\mathbf{n}^\theta)\ e_m^\theta]}{\partial t} d\theta. \tag{6}$$

The equivalent microscopic plastic strain e_m^θ specifies the slip contribution from each orientation θ. Note that the rate of plastic strain $\dot{\mathbf{H}}^p$ is sensitive to the rates of slip $\dot{e}_m^\theta$ and rotations $\dot{\theta}$; these two mechanisms occur in a plastically deformed material. The reorientations include grain rotations, result from the lattice distortions between closely spaced slip bands, are caused by the activation of secondary slip systems, and there is a possibility that some of the plane become curved[19]. These rotations reflect the material's ability for overcoming energy barriers, which are caused by the pre-existing and deformation induced defects. In this manner, the rotations are responsible for the plasticity-induced lattice distortions and cause the storage of energy. The rate of the θ-strain is weighted with $f_\theta(\theta)$, hence $\dot{e}_m^\theta = f_\theta(\theta)\dot{e}_m^p$. The subscript "m" in $\dot{e}_m^p$ indicates that the equivalent strain rate is taken at the microscale. The reorientations (4) are caused by plastic slip and, therefore, we have $\dot{\theta} = (\partial\theta/\partial e_m^\theta)\dot{e}_m^\theta$, hence

$$\dot{\mathbf{H}}^p = \frac{1}{2} \int_{-\pi/4}^{\pi/4} [(\mathbf{n}^\theta\mathbf{s}^\theta + \mathbf{s}^\theta\mathbf{n}^\theta) - 2(\mathbf{n}^\theta\mathbf{n}^\theta - \mathbf{s}^\theta\mathbf{s}^\theta)\ e_m^\theta(\partial\theta/\partial e_m^\theta)\ ]f_\theta(\theta)\ \dot{e}_m^p\ d\theta. \tag{7}$$

We multiply Eq. 7 by the flow tensor $\mathbf{N}^\sigma$. Also, we note that $\mathbf{N}^\sigma:\mathbf{N}^\sigma = 2$ and, therefore, we compare (2) and (7) and conclude that

$$\dot{e}^p = \frac{1}{2}\ \dot{e}_m^p \int_{-\pi/4}^{\pi/4} \mathbf{N}^\sigma: [(\mathbf{n}^\theta\mathbf{s}^\theta + \mathbf{s}^\theta\mathbf{n}^\theta) - 2(\mathbf{n}^\theta\mathbf{n}^\theta - \mathbf{s}^\theta\mathbf{s}^\theta)e_m^\theta(\partial\theta/\partial e_m^\theta)\ ]f_\theta(\theta)d\theta. \tag{8}$$

Next, we express $\mathbf{n}^\theta$ and $\mathbf{s}^\theta$ in reference to $\mathbf{n}^\sigma$ and $\mathbf{s}^\sigma$, where $\mathbf{n}^\theta = \mathbf{n}^\sigma\ \cos\theta + \mathbf{s}^\sigma\ \sin\theta$ and $\mathbf{s}^\theta = \mathbf{s}^\sigma\ \cos\theta - \mathbf{n}^\sigma\ \sin\theta$ and, then

$$\dot{e}^p = \dot{e}^p_m \left[\int_{-\pi/4}^{\pi/4} \cos 2\theta f_\theta(\theta) d\theta - 2 \int_{-\pi/4}^{\pi/4} e^\theta_m (\partial\theta/\partial e^\theta_m) \sin 2\theta f_\theta(\theta) d\theta \right].$$

(9)

The first term in (9) is the rate of plastic strain collected from the current slip systems. The second term represents the contribution of the slip reorientations. The reorientations broaden the distribution $f_\theta(\theta)$ of the available slip systems and, effectively, slow down the flow process. Slip systems that are closely aligned with the direction of maximum shear stress ($\theta = 0$) do not rotate[19,20], while systems at the angles $\theta = \pm \pi/4$ are inactive. As shown[20], the slip reorganizations are maximized somewhere between $\theta = 0$ and $\theta = \pm \pi/4$. For this reason, we propose expression $e^\theta_m (\partial\theta/\partial e^\theta_m) = \alpha^p \sin 2\theta$. Consequently, the strain-induced reorientations become $\tan\theta = \tan\theta_0 (e^\theta_m/e^\theta_0)^{2\alpha^p}$, where the initial slip orientation is θ_0 and the reference plastic strain is e^θ_0. When such a plane is perfectly aligned with the direction of maximum shear stress ($\theta_0 = 0$), then the plane does not rotate. In the case of the misaligned planes ($\theta_0 \neq 0$), the formula reproduces the experimentally observed trends[20]. The rotations increase misalignment of the planes from the direction of maximum shear stress. We realize that an advanced plastic deformation promotes the conditions for the formation of shear bands. Hence, the active planes become realigned with the band's orientations. Accordingly, this realignment is responsible for directional plastic flow. We focus the study on the behavior, where the spectrum of the plane distribution experiences broadening and the plastic flow is isotropic. Consequently, the expression (9) becomes

$$\dot{e}^p = \dot{e}^p_m \left[\int_{-\pi/4}^{\pi/4} \cos 2\theta f_\theta(\theta) d\theta - 2\alpha_p \int_{-\pi/4}^{\pi/4} \sin^2 2\theta f_\theta(\theta) d\theta \right].$$

(10)

Now, we can write $\dot{e}^p = M\dot{e}^p_m$, where the average Schmid factor is $M = M_s - M_r$. From (10), we have $M_s = \int_{-\pi/4}^{\pi/4} \cos 2\theta f_\theta(\theta) d\theta$ and $M_r = 2\alpha_p \int_{-\pi/4}^{\pi/4} \sin^2 2\theta f_\theta(\theta) d\theta$. After integrating we obtain

$$M_s = \frac{\Gamma^2\left(1 + \frac{1}{2r}\right)}{\Gamma\left(\frac{1}{2} + \frac{1}{2r}\right)\Gamma\left[\frac{1}{2}\left(3 + \frac{1}{r}\right)\right]}$$

$$M_r = \alpha_p \frac{\Gamma\left(1 + \frac{1}{2r}\right)}{\Gamma\left(2 + \frac{1}{2r}\right)}$$

(11)

As plastic deformation advances, less favorably oriented systems are activated. The factor M_s quantifies these contributions. The reorientations M_r results from direct interactions of the active systems. The reconfigurations reduce the average Schmid factor and further broaden the spectrum of the plane orientations. When slip is perfectly aligned with the direction of maximum shear stress ($r \to 0$), then the average Schmid factor M is equal to one and $\delta e^p = \delta e^p_m$, Fig. 1. On the other hand, a uniform distribution of slip contributions ($r \to \infty$) maximizes the flow constraints. The exponent r evolves as microscopic plastic strain increases $r = r(e^p_m)$. In the simplest scenario, we make the shape of the distribution dependent on temperature and plastic strain and, therefore, we write $r = A_D\, r_0\, (1 + \varsigma)$ and $\varsigma = e^p_m/e^p_0$ while e^p_0 is a material constant. At high temperatures, the activation factor A_D is a small number and, then, the materials exhibits low resistance plastic flow.

Stability of microstructural evolution.

From the requirement of measure invariance (independence from the frame of description) we write $\boldsymbol{\sigma}: \dot{\mathbf{H}}^p = \sigma_{eq}\dot{e}^p$, where the equivalent stress $\sigma_{eq} = \boldsymbol{\sigma}: \mathbf{N}^\sigma/2$ is maximum shear stress. From (10), the rate of plastic work becomes $\dot{W}^p = (M_s - M_r)\sigma_{eq}\dot{e}^p_m$. The rate of total plastic work is $\dot{W}^p_t = M_s\sigma_{eq}\dot{e}^p_m$ and the portion $\dot{W}^p_r = M_r\sigma_{eq}\dot{e}^p_m$ is retained as internal energy. This mechanism is traditionally known as the stored energy of cold work. The capacity for storing this energy is evolving in the plastically deformed material. In terms of Helmholtz energy, the first order energy perturbation around equilibrium is $\delta F = \delta U|_{r=const} - \delta W^p$, where $\delta U|_{r=const}$ is the change of internal energy calculated in the reference configuration of the slip systems. We narrow down the analysis to conditions, where heat flux can be neglected. Hence, the perturbation becomes

$$\delta F = \delta U|_{r=const} + \sigma_{eq}\delta e^p_m(M_r - M_s).$$

(12)

The material exhibits stable microstructural reconfigurations when $\delta_r(\delta F) > 0$. This condition is satisfied as long as

$$\delta_r(\delta F) = \sigma_{eq}\, \delta e^p_m\, Z\, \delta r \geq 0,$$

(13)

where the variable Z is $\partial(M_r - M_s)/\partial r$. Now, we are ready to introduce the variable $Z_r = \partial M_r/\partial r$, which quantifies the rate of plastic work that is stored in the evolving ensemble of slip systems. The available experimental data suggests that plastic deformation slows down the storage[11]. The condition (13) suggests that a homogeneous deformation produces stable microstructural reconfigurations. The homogeneity can be violated when localized shear bands are formed ($Z\,\delta r < 0$), or the material experiences other damages. The formation of localized shear bands promotes realignment of slip systems. In such a case, the parameter α_p should take negative values. This condition can be constructed by assuming that the parameter α_p is a function of plastic strain and it takes negative

Elasticity		Thermal Activation				Average Schmid Factor			Power-Law Viscoplasticity			
μ	B	k_a	g_a	T_c	T_m	r_0	e_0^p	α_p	σ_0	n_p	ω_p	$\dot{e}_D^0$
MPa	MPa	–	–	K	K	–	mm/mm	–	MPa	–	–	1/s
8110^3	12510^3	2/3	2/3	530	1600	0.1	0.013	$2.56/\pi$	550	1	0.98	510^{-6}

Table 1. Material constants for steel 304L.

values at a critical state of plastic deformation. Also, a strong dynamic excitation may trigger unstable microstructural evolution. We paraphrase the argument by Prigogine[21] and state that the instability results from the interplay of three aspects which are always linked in a dissipative material: there is the mechanism of inelastic flow, there are the microstructural reconfigurations, and there are the flow fluctuations, which trigger the instability. The role of such fluctuations in a plastically deformed material has been discussed in ref. 22.

Power-law viscoplasticity. In our approach, the rate of the microscopic plastic strain is expressed in terms of the current stress. We propose a power-law constitutive relation, which couples the rate of the micro-plastic equivalent strain with the equivalent stress

$$\dot{e}_m^p = \dot{\Lambda}_p \left(\sigma_{eq}/\sigma_0^p \right)^{n_p}. \tag{14}$$

Strength σ_0^p is a temperature sensitive quantity and, therefore, the actual strength is $\sigma_0^p = \sigma_0 A_D$, while the athermal strength σ_0 is a material constant. We correct the power-law rate relation in (14) and introduce a rate-sensitive factor $\dot{\Lambda}_p = \dot{e}_N^0 \left[\dot{e}_N^t/\dot{e}_N^0 + (\dot{e}_D/\dot{e}_N^0)^{1/1-A_D} \right]^{\omega_p}$, where $\dot{e}_N^t = 4\, n_p (\dot{\mathbf{H}}^t : \dot{\mathbf{H}}^t)^{1/2}$, the parameter $\dot{e}_N^0 = 1/s$ is the reference rate, and $\dot{\mathbf{H}}^t$ is the rate of total strain. The term $(\dot{e}_D/\dot{e}_N^0)^{1/1-A_D}$ describes the contribution of diffusional flow, where the parameter $\dot{e}_D$ is a constant and is in the order of $10^{-6}/s$. The function A_D has already been derived (Eqn. 1) and the exponent ω_p is a constant slightly smaller from one. At high temperatures and/or very low strain rates, the term $(\dot{e}_D/\dot{e}_N^0)^{1/1-A_D}$ affects the flow process defined in (14). At the initial stage of plastic deformation, the rate of elastic strain dominates ($\dot{\mathbf{H}}^e \rightarrow \dot{\mathbf{H}}^t$) and, therefore, we have $\dot{e}_m^p \propto (\sigma_{eq}^p/\sigma_0^p)^{n_p}$. When the rate of plastic strain controls the deformation process ($\dot{\mathbf{H}}^p \rightarrow \dot{\mathbf{H}}^t$), the strain rate sensitivity is $\dot{e}_m^p \propto (\sigma_{eq}^p/\sigma_0^p)^{n_p/(1-\omega_p)}$. Consequently, the material experiences a smooth strain rate transition from $\dot{e}_m^p \propto (\sigma_{eq}^p/\sigma_0^p)^{n_p}$ to a nearly strain rate insensitive plastic flow $\dot{e}_m^p \propto (\sigma_{eq}^p/\sigma_0^p)^{n_p/(1-\omega_p)}$. In this construction, the model captures diffusional flow, power-law creep and plasticity. It is worth mentioning that similar power-law expressions have already been used for metals[23,24] and frictional materials[25]. Elastic material properties complete the constitutive description. We use the rule of the strain rate additivity $\dot{\mathbf{H}}^t = \dot{\mathbf{H}}^e + \dot{\mathbf{H}}^p$ and, then, the rate of stress is $\dot{\boldsymbol{\sigma}} = \mathbf{C} \cdot \dot{\mathbf{H}}^e$, where the fourth order elastic tensor is $\mathbf{C}$.

Discussion

Model validation. We have four groups of independently verifiable parameters. First group constitutes elastic properties (μ, B). The second describes the thermally activated processes (k_a, g_a, T_c, T_m). The average Schmid factor is defined in terms of two parameters (r_0, e_0^p) and, then, the rate of slip reconfigurations is controlled by the parameter α_p. Lastly, the power-law flow rules are determined in terms of four parameters $\left(\sigma_0, n_p, \omega_p, \dot{e}_D^0 \right)$. The thermally activated processes are calibrated against experimental data, where yield stress is plotted as a function of temperature. The average Schmid factor controls the rate of plastic hardening and the rate of the energy storage. The flow rules determine the stress-strain rate sensitivity. We calibrate the model for stainless steel 304L and the parameters are listed in the Table 1. The model is coded and figures are constructed using the Wolfram software Mathematica. First, we compare the predicted and experimentally obtained stress-strain responses at strain rate 0.66/s and room temperature, Fig. 2. Red dots in the plot represent the experimental data. We also show the material's sensitivity to strain rates ranging from $6.610^{-5}/s$ to 66.0/s. On the same plot, we include the normalized yield stress plotted as a function of temperature. Yield stress is normalized with respect to yield at room temperature. Again, the dots represent published experimental data[26–28]. Both the predictions in Fig. 2 are matching the experimental data, though it is understandable that the data gathered from multiple sources exhibits some scatter. Next, we compare the experimentally measured rate of the energy storage and compare it with our predictions $Z_r = \partial M_r/\partial r$, Fig. 3. The scatter of measurements results from the heat fluctuations, which occur both in time and space. Such fluctuations are caused by stochasticity of the dislocation multiplication, motion and storage. Similar responses are obtained for 2024-T3 aluminum alloy and α-titanium; both of the materials are subjected to quasi-static and dynamic loading[29]. In all the cases[29–31], the rate of storage decreases as the material is plastically deformed. Our model correctly predicts the slowdown of the storage. As we indicated earlier, the formation of shear bands should reverse the trends. The power-law viscoplasticity captures the behaviors from diffusional flow, power-law creep up to the plastic flow. We demonstrate these deformation mechanisms by constructing the Frost-Ashby deformation map[32], Fig. 4. Our map captures the main features of the behavior within a broad range of strain rates and temperatures.

Our motivation has been to capture the relevant micro-mechanisms of plastic flow, while retaining the simplicity of the phenomenological material description. In this manner, we bridge the phenomenology with the relevant mechanisms of plastic deformation. We do not identify independent crystallographic orientations and, instead, apply weight to each θ orientation. Thus, in our approach slip occurs along a broad spectrum of planes
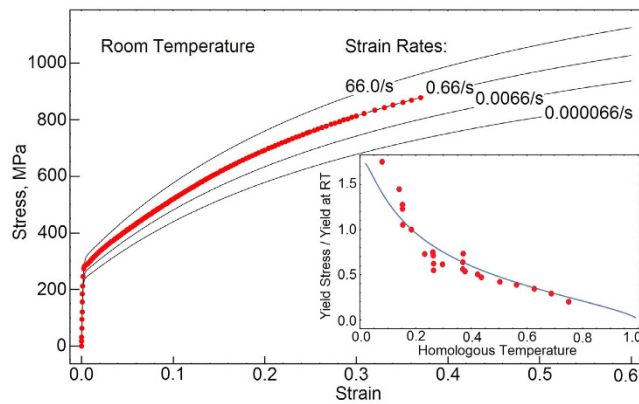
Figure 2. Uniaxial stress versus strain in tension is plotted for four different strain rates and at room temperature. Red dots represent experimental data. The embedded plot shows yield stress constructed in terms of temperature. The prediction is compared with experimental data gathered from refs 26–28.
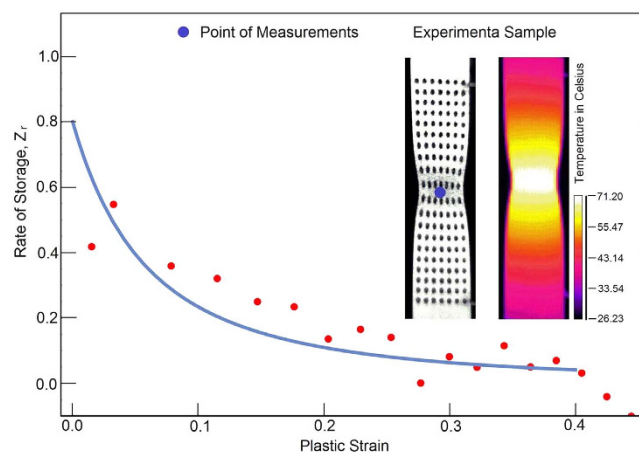

Figure 3. The rate of energy storage is plotted as a function of plastic strain. Red dots represent our experimental data obtained from the simultaneous measurements of infrared and visible cameras.

and, then, the plastic flow is projected onto the plane of maximum shear stress. The slip reconfigurations are detectable in our measurements of the energy storage rate. We have shown that these reconfigurations are stable in a homogeneously deformed material. However, the processes may become unstable in the presence of localized shear bands. The latter are triggered by strong spatial and temporal stress fluctuations discussed in ref. 22. We complete the approach by introducing the description for the thermally activated motion of dislocations, where two characteristic temperatures are introduced. The transition temperature T_c differentiates the behavior between the power-law creep mechanism and the low-rate sensitive dislocation glide. The melting temperature T_m is introduced for a proper description of diffusional flow. Also, we propose a generalized model for the power-law flow, where we capture the inelastic behaviors associated with diffusional flow, power-law creep and plasticity. We validate the approach by developing a constitutive model for stainless steel 304L. The material's chemical composition is designed for impeding the deformation-induced martensitic transformation.

Methods
Experimental procedure. As mentioned above, a part of the plastic work is dissipated as heat and the rest of it increases internal energy. In the area of the strain localization, the distribution of the strain rates is not uniform and, therefore, a non-uniform temperature field is observed on the surface of the specimen[31]. Evolution of the temperature field during the deformation process is recorded by a high sensitivity IR thermography system. The average temperature of the selected section of the specimen is plotted as a function of time. Note that the section is positioned in such a manner to avoid the influence of the specimen edges on the measured temperature values. The initial volume of the section is equal to $(1.3 \times 1.3 \times 2)$ mm^3 and the initial cross-section is (1.3×2) mm^2. The size of the section is changing during the tensile deformation. These changes are monitored by tracking the section's center in the visible range by means of the CCD camera. All these data have been used to calculate heat generated during short time interval in the section. The interval is the reciprocal of the measurement frequency. The experiments are performed on austenitic stainless steel with chemical composition shown in Table 2. This composition is developed to mitigate the phase transformation during the deformation process. The strips with
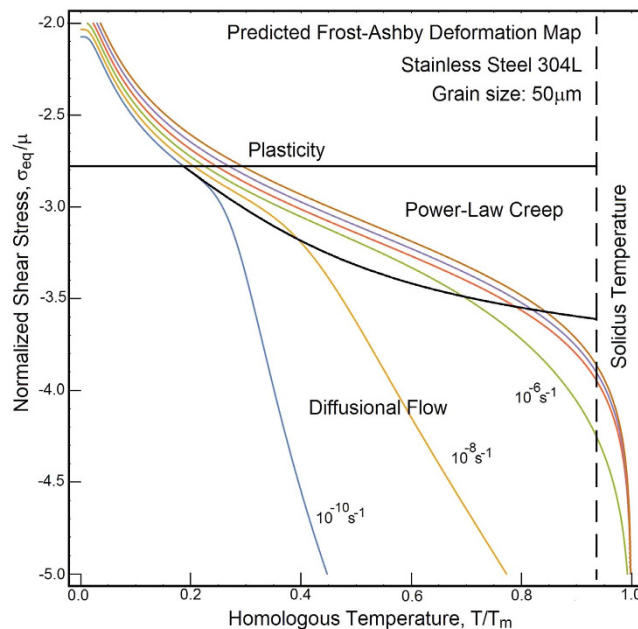
Figure 4. The mechanisms-based model is used for the prediction of the Frost-Ashby deformation map for stainless steel 304L (ref. 32, p. 66). The chemical composition of the steel is presented in Table 2. Solid lines represent the material responses at constant strain rate plotted as a function of the normalized shear stress and homologous temperature.

C	Mn	Si	P	S	Cr	Ni	W	Mo	Cu	V	Ti	Fe
0.05	1.35	1.0	0.016	0.008	18.58	17.3	0.025	0.02	0.04	0.03	0.013	Balance

Table 2. Chemical composition (wt. %).

the cross-section $25\,mm \times 4\,mm$ are initially annealed at $1{,}050\,°C$, water quenched and 50% cold rolled. Then, the specimens for tensile testing are cut to the right shape using an electro-erosion machining. Prior to testing, the specimens are annealed for 1 h at $1{,}100\,°C$ and water quenched to produce a homogeneous microstructure with a mean grain size about $50\,\mu m$ and are electro-polished. We use MTS 858 testing machine and apply tensile deformation with the displacement rate, which corresponds the strain rate equal to 0.66/s. In the course of the deformation process, the infrared and visible range image sequences are recorded simultaneously using the infrared Phoenix and pco. 1200 hs cameras. The measurement frequency of both cameras is equal to 538 Hz. This frequency is sufficient to avoid the contribution of heat transfer between neighboring sections. The analysis of the displacement field (based on markers tracking) and the appropriate temperature distributions is performed using MATLAB software.

References

1. McDowell, D. L. Viscoplasticity of heterogeneous metallic materials. *Mat. Sci. Eng. R* **62,** 67–123 (2008).
2. Taylor, G. & Quinney, H. The latent energy remaining in a metal after cold working. *Proc R. Soc. Lond.* **143,** 307–326 (1934).
3. Wolfenden, A. The ratio of stored to expended energy during the deformation of copper and aluminium single crystals at 78 K. *Acta Metall.* **16,** 975–980 (1968).
4. Chrysochoos, A. & Maisonneuve, O. Energy balance for elastic plastic deformation at finite strain. *C.R. Acad. Sci.* **300,** 985–990 (1985).
5. Oliferuk, W., Świątnicki, W. & Grabski, M. W. Rate of energy storage and microstructure evolution during the tensile deformation of austenitic steel. *Mater. Sci. Eng. A* **161,** 55–63 (1993).
6. Hodowany, J., Ravichandran, G., Rosakis, A. J. & Rosakis, P. Partition of plastic work into heat and stored energy in metals. *Exp. Mech.* **40,** 113–123 (2000).
7. Oliferuk, W. & Maj, M. Stress–strain curve and stored energy during uniaxial deformation of polycrystals. *Eur. J. Mech. A/Solids* **28,** 266–272 (2009).
8. Rönnpagel, D. & Schwink, C. H. Measurement of the stored energy of copper single crystals by means of a new deformation calorimetry method. *Acta Metall.* **26,** 319–331 (1978).
9. Oliferuk, W., Gadaj, S. P. & Grabski, M. W. Energy storage during the tensile deformation of Armco iron and austenitic steel. *Mater. Sci. Eng.* **70,** 131–141 (1984).
10. Rittel, D. On the conversion of plastic work to heat during high strain rate deformation of glassy polymers. *Mech. Mater.* **31,** 131–139 (1999).
11. Rosakis, P., Rosakis, A. J., Ravichandran, G. & Hodowany, J. A thermodynamic internal variable model for the partition of plastic work into heat and stored energy in metals. *J. Mech. Phys. Solids* **48,** 581–607 (2000).
12. Bever, M. B., Holt, D. L. & Titchener, A. L. The stored energy of cold work. *Prog. Mater. Sci.* 17, 23–58, Pergamon Press (1973).
13. Asaro, J. R. Crystal Plasticity. *J. Appl. Mech.* **50,** 921–934 (1983).

14. Nemat-Nasser, S. & Okinaka, T. A new approach to crystal plasticity: fcc single crystal, *Mech. Mat.* **25,** 43–57 (1996).
15. Anand, L. & Kothari, M. A computational procedure for rate-independent crystal plasticity. *J. Mech. Phys. Solids* **44,** 525–558 (1996).
16. Ryu, S., Kang, K. & Cai, W. Entropic effect on the rate of dislocation nucleation. *PNAS* **108,** 5174-5178 (2011).
17. Zubelewicz, A. Micromechanical study of ductile polycrystalline materials. *J. Mech. Phys. Solids* **41,** 1711–1722 (1993).
18. Borbely, A., Maurice Piot, D. & Driver, J. H. Spatial characterization of the orientation distribution in a stable plane strain-compressed Cu crystal: A statistical analysis. *Acta Mat.* **55,** 487–496 (2007).
19. Di Gioacchino, F. & Quinta da Fonseca, J. An experimental study of the polycrystalline plasticity of austenitic steel. *Int. J. Plast.* **74,** 92–109 (2015).
20. Pantheon, W. Distribution in dislocation structures: Formation and spatial correlation. *J. Meter. Res.* **17,** 2433–2441 (2002).
21. Prigogine, I. Time, structure and fluctuations. *Nobel Lecture* Dec. 8, 1997.
22. Zubelewicz, A. Metal behavior at extreme loading rate: Thermodynamics. *Phys. Rev.* B **77,** 214111 (2008).
23. Zubelewicz, A., Zurek, A. K. & Potocki, M. L. Dynamic behavior of copper under extreme loading rates. *J. Phys. IV* **138,** 23–27 (2006).
24. Zubelewicz, A., Addessio, F. & Cady C. Constitutive Model for Uranium-Niobium Alloy. *J. Appl. Phys.* **100,** 013523 (2006).
25. Zubelewicz, A. *et al.* Dynamic behavior and fracture of materials. *Int. J. Rock Mech. and Mining Sci.* **72,** 277–282 (2014).
26. Towfighi, S., Romilly, D. P. & Olson, J. A. Elevated temperature material characteristics of AISI 304L stainless steel. *Mat. High Temp.* **30,** 151–156 (2013).
27. Blandford, R. K., Morton, D. K., Snow, S. D. & Rahl, T. E. Tensile stress-strain results for 304L and 316L stainless steel plate at temperature. *Proc. ASME 2007 Pressure Vessels and Piping Conf.* 6, 617–628, San Antonio, TX, July 22-26 (2007).
28. Weon Kim, J. & Sang Byun, T. Analysis of tensile deformation and failure in austenitic stainless steels: Part I–Temperature dependence. *J. Nucl. Mat.* **396** (1–9) (2010).
29. Hodowany, J., Ravichandran, G., Rosakis, A. J. &Rosakis, P. Partition of plastic work into heat and stored energy in metals, *Exp. Mech.* **40,** 113–123 (2000).
30. Oliferuk, W., Maj, M. & Raniecki, B. Experimental analysis of energy storage rate components during tensile deformation of polycrystals. *Mat. Sci. Eng. A,* **374,** 77–81 (2004).
31. Oliferuk, W., Maj, M. & Zembrzycki, K. Determination of the energy storage rate distribution in the area of strain localization using infrared and visible imaging. *Exp. Mech.* **55,** 753–760 (2015).
32. Frost, H. & Ashby, M. F. *Deformation-mechanism maps: The plasticity and creep of metals and ceramics.* Pergamon Press, Oxford (1982).

Acknowledgements

Author Contributions

A.Z. developed the mechanisms-based concept and constructed constitutive model for steel 304L. W.O. provided experimental data suitable for calibration of the model. All authors reviewed the manuscript.

Additional Information

Competing financial interests: The authors declare no competing financial interests.

How to cite this article: Zubelewicz, A. and Oliferuk, W. Mechanisms-based viscoplasticity: Theoretical approach and experimental validation for steel 304L. *Sci. Rep.* **6**, 23681; doi: 10.1038/srep23681 (2016).